# Enhanced Thermal Stability of Conductive Mercury Telluride Colloidal Quantum Dot Thin Films using Atomic Layer Deposition

Edward W Malachosky , Matthew M Ackerman * , Liliana Stan

Posted Date: 17 July 2024

doi: 10.20944/preprints202407.1429.v1

Keywords: atomic layer deposition; colloidal quantum dots; shortwave infrared; CQD; ALD; thermal stability; photodetector; mercury telluride; HgTe

*Article*

# Enhanced Thermal Stability of Conductive Mercury Telluride Colloidal Quantum Dot Thin Films Using Atomic Layer Deposition

**Edward W. Malachosky [1], Matthew M. Ackerman [1,*] and Liliana Stan [2]**

[1] QDIR, Inc., 3440 S. Dearborn St. Suite 114S, Chicago, IL 60616, USA; ewmalachosky@qdinfrared.com
[2] Argonne National Laboratory - Center for Nanoscale Materials, Lemont, IL, 60439 USA; lstan@anl.gov
* Correspondence: mackerman@qdinfrared.com

**Abstract:** Colloidal quantum dots (CQDs) are valuable for their potential applications in optoelectronic devices. However, they are susceptible to thermal degradation during processing and while in use. Mitigating thermally induced sintering, which leads to absorption spectrum broadening and undesirable changes to thin film electrical properties, is necessary for the reliable design and manufacture of CQD-based optoelectronics. Here, low temperature metal-oxide atomic layer deposition (ALD) was investigated as a method for mitigating sintering while preserving the optoelectronic properties of mercury telluride (HgTe) CQD films. ALD-coated films are subjected to temperatures up to 160°C for up to 5 hours and alumina ($Al_2O_3$) is found to be most effective at preserving the optical properties, demonstrating the feasibility of metal-oxide infilling to protect against sintering. HgTe CQD film electrical properties were investigated before and after alumina ALD in-filling, which was found to increase the p-type doping and hole mobility of the films. The magnitude of these effects depended on the conditions used to prepare the HgTe CQDs. With further investigation into the interaction effects of CQD and ALD process factors, these results may be used to guide the design of CQD-ALD materials for their practical integration into useful optoelectronic devices.

**Keywords:** atomic layer deposition; colloidal quantum dots; shortwave infrared; CQD; ALD; thermal stability; photodetector; mercury telluride; HgTe

## 1. Introduction

Colloidal quantum dots (CQDs) are of great interest for optoelectronics including light emitting devices [1], energy harvesting photovoltaics [2], solar concentrators [3], and photodetectors [4]. However, when subjected to elevated temperatures that can occur during manufacturing, testing, or while in use, CQDs and their device performance can degrade. One mode of degradation is thermal sintering, during which neighboring CQDs fuse together. Sintering occurs at elevated temperatures as the activation barrier to ion diffusion is overcome and interfaces can reconstruct to reduce the high surface energy of the CQDs. Consequently, quantum confinement is lost during sintering, causing broadening of the absorption spectrum and harmful changes to the electrical properties of the films.

A common solution to this problem is to grow a shell on the surface of the CQDs to prevent neighboring core materials from fusing together. Such a core-shell structure has been most successful for light emitting and display technologies. However, the shell is typically designed to confine the charge carriers rather than to promote charge separation. This effect of the shell impedes carrier extraction, making the approach impractical for photovoltaic and photodetector devices. Therefore, a method other than a shell is needed for the practical development of CQD-based, charge-collecting devices.

In bulk semiconductor devices, metal oxides and nitrides have been used to protect the integrity of the active elements and interconnects from metal ion diffusion at elevated process temperatures

 doi:10.20944/preprints202407.1429.v1



and during operation [5]. Such diffusion barriers may also prevent sintering between neighboring colloidal quantum dots without preventing charge transport, if such a diffusion barrier could be grown within the CQD thin film. Low-temperature atomic layer deposition (ALD) has been used to fill the spaces in CQD films with metal oxides, leading to improved charge carrier transport and providing protection against oxidation for air-stable PbX (X=S,Se) [6,7] and InP CQDs [8]. However, the impact of in-filled ALD metal oxides on the thermal stability of CQD solids has not yet been reported.

Here, metal oxides as barriers were prepared by low-temperature ALD on conductive HgTe CQD solid films. Zinc oxide (ZnO), titanium dioxide ($TiO_2$), and alumina ($Al_2O_3$) were readily available and evaluated as barrier materials against thermally induced sintering. The optical and electronic properties were evaluated to determine the effectiveness of the respective barrier material against sintering before and after subjecting the ALD-coated HgTe CQD thin films to elevated temperatures.

## Materials and Methods

*Preparation of Trioctylphosphine Telluride (TOPTe)*

A stock solution of 1 M tellurium precursor was prepared by dissolving tellurium shot in trioctylphosphine (TOP) at 100°C overnight in a nitrogen filled glovebox.

*Synthesis and Post-Synthesis Processing of p-Type HgTe Colloidal Quantum Dots*

For p-type HgTe colloidal quantum dots, the procedure was adapted from Ackerman, *et al*. [10]. In a typical synthesis, 54 mg (0.1 mmol) of $HgCl_2$ and 10 mL oleylamine were transferred to a 50 mL round bottom flask. The reaction solution was left to mix at 100°C under nitrogen flow for 1 hour. The reaction temperature was reduced to 85°C. Then, 0.2 mL of TOPTe was diluted in 10 mL oleylamine (10 mL), and the mixture was rapidly injected into the round bottom flask. The reaction was allowed to proceed for 1 to 10 minutes before quenching with 10 mL of tetrachloroethylene and cooling to room temperature. A 1 mL addition of 1-dodecanethiol was added to the solution, followed by precipitation once with ethanol. The supernatant was discarded, and the pellet dissolved in 10 mL of chlorobenzene. A white gel was present on the surface of the solution, and a 1 mL fraction of TOP was added to remove this gel. The solution was again precipitated with ethanol and re-dissolved in chlorobenzene. No white gel was observed after the addition of TOP and the second precipitation. The solution was stored in ambient until further use.

HgTe CQDs were cleaned with dodecylethyldimethylammonimum bromide (DEDAB) (0.1 M in isopropanol) and isopropanol (IPA), and then dissolved in a mixture of chlorobenzene and butyl acetate. Thin films were drop-casted at 40°C under ambient conditions onto sapphire substrates for thin film absorption measurements or on interdigitated electrodes for electrical measurements. Thin films were then crosslinked for 30 seconds by soaking in an ethanedithiol(1%)/hydrochloric acid(1%)/IPA solution, followed by rinsing with neat IPA and blown dry with compressed air.

*Synthesis and Post-Synthesis Processing of n-Type HgTe Colloidal Quantum Dots*

For n-type HgTe colloidal quantum dots, the procedure was adapted from Yang *et al*. [9]. In a typical synthesis, 180 mg (0.66 mmol) of $HgCl_2$ and 10 mL of oleylamine were transferred to a 50-mL round bottom flask. The mixture was heated at 100 °C for 1 hour under vacuum to fully dissolve $HgCl_2$. The temperature was reduced to 80°C, vacuum was closed, and nitrogen flow was opened for the reaction. Then, a premixed solution of 200 µL of TOPTe, 50 µL of 1-dodecanethiol, and 800 µL of oleylamine was quickly injected into the $HgCl_2$ solution. After 1 minute, a second premixed solution of 200 µL of TOPTe in 800 µL of oleylamine was added dropwise over 2 minutes. The reaction proceeded for another 3 minutes and then was quenched with 10 mL of tetrachloroethylene. The heating mantle was replaced with a water bath to further cool to room temperature. At a temperature less than 30°C, 0.6 mL of 3-mercaptopropionic acid was injected and left to mix under nitrogen for 1

 doi:10.20944/preprints202407.1429.v1



hour. The HgTe CQDs were then precipitated with isopropanol. The clear supernatant was discarded and the HgTe CQDs were stored in octane in a nitrogen glovebox until further use.

To prepare the n-type HgTe CQDs for coating, a phase transfer process was used to control lock-in the n-type doping. Typically, 180 mg (0.66 mmol) $HgCl_2$, 140 µL of 2-mercaptoethanol and 400 µL of n-butylamine were pre-dissolved in 5 mL of dimethylformamide (DMF). Then, 1 mL of the DMF solution was transferred to a centrifuge tube along with 1 mL of the HgTe CQD in octane stock solution. The phases were mixed for 1 minute and allowed to separate, after which the HgTe CQDs had transferred to the DMF phase. The octane phase was removed, followed by washing 3 times with 1 mL of neat octane to residual non-polar materials. Once the last octane washing phase was removed, HgTe CQDs in DMF were precipitated by the addition of 1 mL of toluene. The clear supernatant was discarded and the HgTe CQDs were redispersed with 200 µL of DMF to obtain concentrated ink. The ink was blade coated at 60°C onto sapphire substrates for FTIR measurements or interdigitated electrodes on doped silicon substrates for conductance and FET measurements. Thin films were then crosslinked for 30 seconds by soaking in an ethanedithiol(1%)/hydrochloric acid(1%)/IPA solution, followed by rinsing with neat IPA and blown dry with compressed air.

*Atomic Layer Deposition on Colloidal Quantum Dot Thin Films*

ALD infill of HgTe CQD films presented in this paper was performed using an Arradiance Gemstar benchtop system. The metal precursors used were trimethylaluminum (TMA) for $Al_2O_3$, diethyl zinc (DEZ) for ZnO, and tetrakis(dimethylamino)titanium (TDMAT) for $TiO_2$. Water was used as an oxidant for all films. High exposure mode ALD processes, having two half cycles were used. A half cycle consisted of precursor injection in a series of short pulses, followed by an exposure time, and then a purging step. During the high exposure-mode ALD process, the evacuation valve was closed before introducing the precursor in the chamber and opened after the exposure time. N2 was used as a carrier and purging gas. The experimental parameters are listed below:

| | **ALD Material** | $Al_2O_3$ | ZnO | $TiO_2$ |
|---|---|---|---|---|
| | **Metal precursor** | TMA | DEZ | TDMAT |
| | **Reactant** | Water | Water | Water |
| | **Temperature** | 80 C | 80 C | 80 C |
| **1st half cycle (metal precursor)** | **N2 flow** | 5 sccm | 10 sccm | 10 sccm |
| | **Metal precursor pulse time** | 150 ms | 80 ms | 700 ms |
| | **pulse delay** | 10 s | 10 s | 10 s |
| | **Number of pulses** | 6 | 6 | 6 |
| | **exposure time** | 600, 1200 s | 400 s | 120 s |
| | **purge time** | 90 s | 90 s | 240, 480 s |
| **2nd half cycle (water)** | **N2 flow** | 5 sccm | 10 sccm | 5 sccm |
| | **Water pulse time** | 80 ms | 80 ms | 80 ms |
| | **water pulse delay** | 10 s | 10 s | 10 s |
| | **Number of water pulses** | 6 | 6 | 6 |
| | **exposure time** | 400, 800 s | 400 s | 240 s |
| | **purge time** | 120 s | 120 s | 240, 480 s |
| | **Number of cycles** | 4, 8, 20 | 8 | 20 |

*Characterization of Optical Properties*

Absorption spectra of HgTe colloidal quantum dot thin films were made using a Nicolet 550 FTIR. Samples were measured in transmission mode. The sample, consisting of a HgTe CQD thin film (with and without ALD) on a sapphire substrate, was placed in the beam path in the sample chamber such that the sapphire surface was oriented with a 45° tilt with respect to the incident beam path. The sample tilt was necessary to minimize interference effects—due to the different indices of

 doi:10.20944/preprints202407.1429.v1



the CQD and sapphire substrate in the optical path—while preserving the lineshape of the CQD thin film absorption.

*Conductance and Field Effect Transistor Measurements*

Conductance and field effect transistor (FET) measurements were made using substrates consisting of Au-Au interdigitated electrodes on a doped silicon/silicon dioxide substrate. Gold (Au) interdigitated electrodes (30 pairs, each pair have a 5 μm channel width and 1 mm finger length) were patterned by photolithography and e-beam deposition of Ti(20 nm)/Au(80 nm) on n++ doped silicon substrate with 300 nm silicon dioxide surface layer. The doped silicon substrate and 300 nm silicon dioxide layers served as the backside gate and insulator, respectively, in the thin film field effect transistor. For conductance measurements, the silicon backside gate was left open and electrically insulated from the surface conductor. For FET measurements, a 1 V bias was applied between the source-drain interdigitated contacts while a variable gate bias ($V_g$) was applied to the silicon backside gate. The conductor or FET samples were placed on the probe station stage and aluminum wire probes were brought into electrical contact with the source, drain, and gate contacts. A Keithley 4200 parameter analyzer was used to program source, drain, and gate biases and to measure the conductor current or FET source-drain current as a function of gate voltage, respectively. All measurements were carried out at room temperature under ambient conditions.

**Result and Discussion**

Thin films of HgTe CQDs were coated onto sapphire substrates and in-filled by ALD with different metal oxides. Infrared-transparent sapphire was selected as the substrate to facilitate FTIR absorption measurements before and after ALD and high-temperature baking. The amount of the metal oxide deposited was controlled by the number of cycles and dwell time of the precursor gases.

**Figure 1** shows the evolution of the HgTe CQD infrared absorption spectra as a function of ALD deposition and baking conditions for zinc oxide (ZnO), titanium dioxide ($TiO_2$), and alumina ($Al_2O_3$). Both ZnO and $TiO_2$ failed to preserve the exciton absorption feature following ALD such that these materials were deemed to be incompatible with HgTe CQDs as a barrier against thermal sintering. In the case of ZnO (**Figure 1a**), the exciton absorption feature of the HgTe CQDs blue-shifted immediately upon ALD treatment. The spectral shape was maintained with ZnO coating until the baking was increased to 160°C for 5 hours, at which point the exciton absorption feature was completely quenched. For $TiO_2$ (**Figure 1b**), the exciton feature broadened and red-shifted following ALD, then failed to mitigate sintering when baked above 130°C as evidenced by the loss of the exciton feature. The additional peaks found between 2700 and 3000 nm can be assigned to coordinated hydroxyl group residuals at the surface of the ALD deposited oxides, varying in position depending on coordination number and species with respect to Al, Zn, or Ti [11–13].

In contrast, $Al_2O_3$ both preserved the exciton feature overall—suffering a marginal broadening and red-shift—and provided significantly improved thermal stability against sintering compared to ZnO and $TiO_2$. **Figure 1c-e** show the evolution of the absorption spectrum with increasing temperature and increasing number of cycles (4, 8, and 20, respectively) of the alumina on the HgTe CQD. A minor redshift was observed between the control and post-ALD/pre-bake steps that cannot be attributed to thermal effects. Between 8 cycles (**Figure 1d**) and up to 20 cycles (**Figure 1e**) of ALD were sufficient to retain the exciton feature of the absorption spectrum after baking at 130°C for 2 hours and 160°C for 5 hours. This demonstration is evidence that ALD can be used to fabricate barriers that can provide thermal stability against sintering. Further development of alumina—as well as the investigation of other materials such as metal chalcogenides that are commonly used with infrared semiconductors—may lead to the robust design of CQD-based optoelectronics, especially photodetectors.

 doi:10.20944/preprints202407.1429.v1



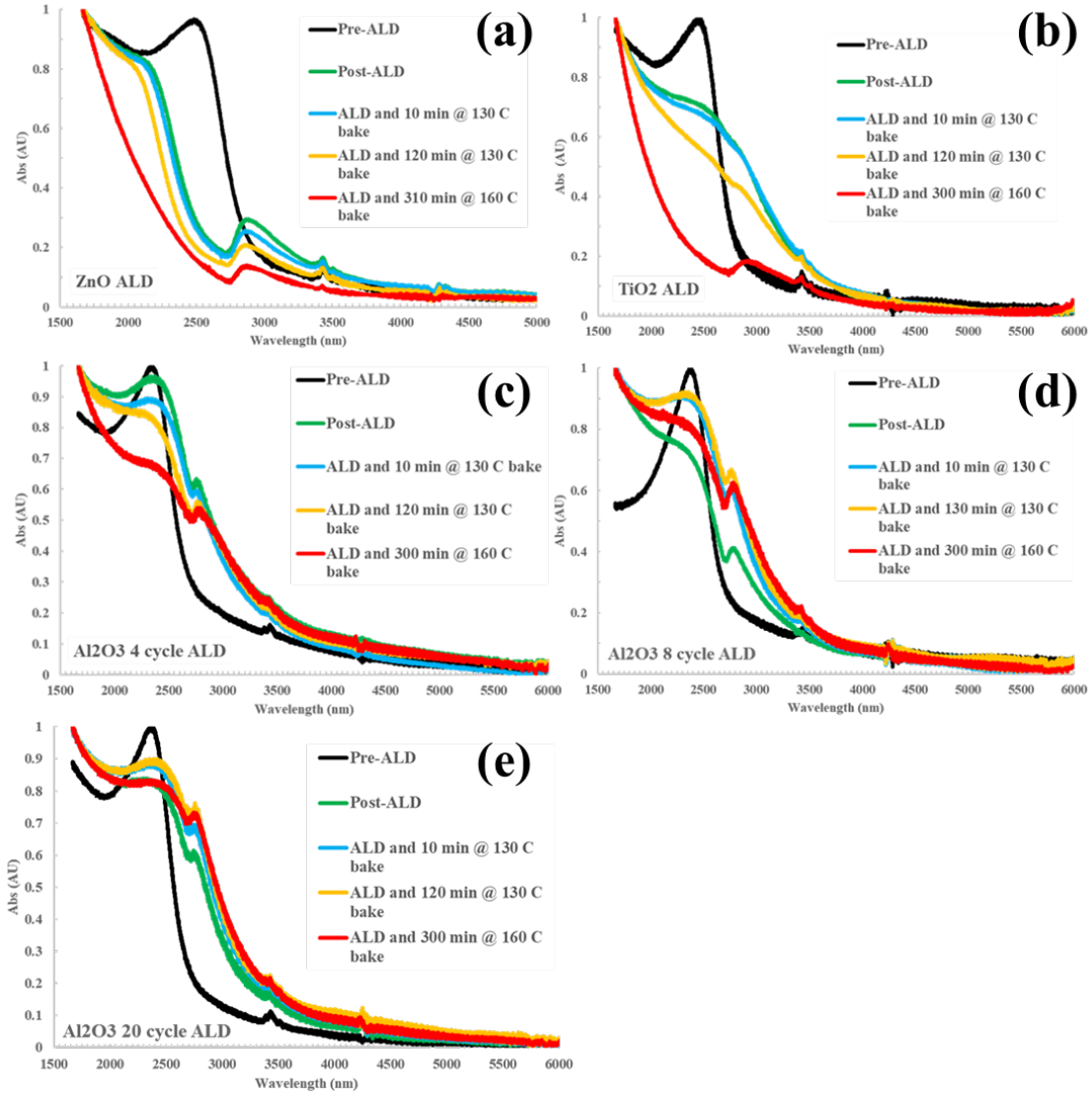


**Figure 1.** Infrared absorption spectra plotted against wavelength (nm) of HgTe CQD thin films on sapphire substrates measured as a function of atomic layer deposition cycles and bake conditions. Evolution of the infrared absorption spectrum for HgTe CQD after (a) ZnO, (b) $TiO_2$, (c) 4 cycles of alumina, (d) 8 cycles of alumina, and (e) 20 cycles of alumina and subjected to baking up to 165°C for up to 5 hours.

Having established the feasibility of ALD as a method for preserving the integrity of the HgTe CQDs, the impact of ALD on the electrical properties of these thin films was investigated. First, simple photoconductor measurements, as shown in **Figure 2**, were used to assess the impact of ALD in-filling on the conductance of HgTe CQD films. Thin films of HgTe CQDs were deposited on gold interdigitated electrodes and then coated with either no alumina (control sample), 8 cycles, or 20 cycles of alumina by ALD. The photoconductors were characterized before and after baking at 130°C for 2 hours. Comparing current levels before baking (**Figure 2a**) and after baking (**Figure 2b**), it was apparent that both 8 and 20 cycle alumina ALD preserved the conducting properties of the HgTe CQD film while un-passivated films degraded, as indicated by the significant increase in current after baking.

 doi:10.20944/preprints202407.1429.v1



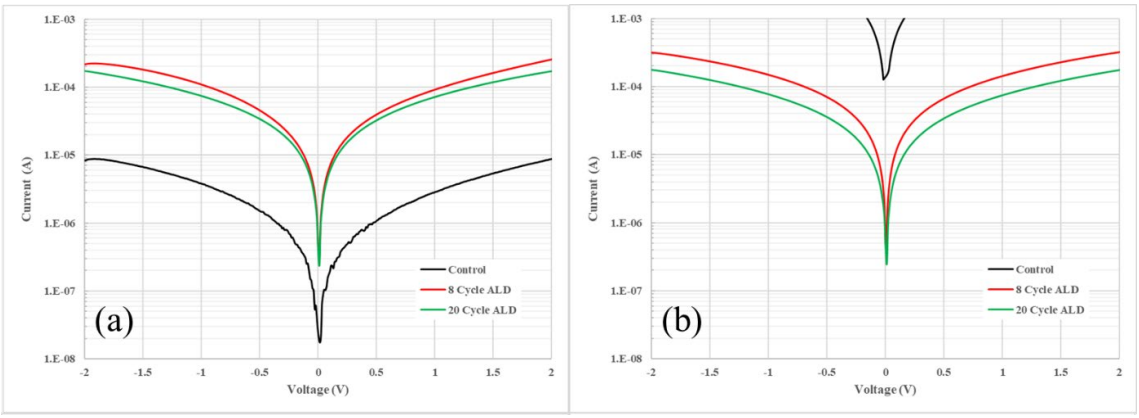


**Figure 2.** Log plots of the current versus voltage for HgTe CQD thin film Au-Au photoconductor devices with a 5 microns electrode gap. The conductance for a control device (black) that was not subjected to atomic layer deposition, a film subjected to 8 cycles of alumina ALD (red), and a film subjected to 20 cycles alumina ALD (green) are plotted for comparison. Conductance of HgTe CQD films measured (a) before and (b) after baking at 130°C for 2 hours under nitrogen environment are shown.

An order-of-magnitude increase in the conductance following ALD coating was also notable in **Figure 2a** before subjecting the films to baking. An increase in the conductance of the CQD film could follow from higher carrier mobility, higher doping density, or both due to ALD in-filling. To investigate what contributed to this change, field effect transistor (FET) measurements were made on HgTe CQD thin films before and after ALD. Samples consisted of HgTe CQD films coated on Au-Au interdigitated electrodes (source and drain) patterned on a heavy n-type doped silicon substrate (gate) with a 300 nm $SiO_2$ dielectric layer. Measurements were made across multiple FET devices.

The transfer curves, shown in **Figure 3**, were measured before (**Figure 3a**) and after (**Figure 3b**) alumina ALD and analyzed to understand the impact of ALD on the mobility and doping the HgTe CQD thin films. Before ALD (**Figure 3a**), the average minima of conductance were at gate voltages ($V_g$) between 0 V and +5 V, which suggests near-intrinsic to light p-type doping, respectively, of the thin films. After ALD (**Figure 3b**), the minima of conductance were greater than +30 V and not observable on the scale of the measurement, suggesting a shift to heavy p-type doping of the thin films following ALD coating.

With respect to carrier transport, the carrier mobilities were estimated by taking the slopes indicated by the dashed lines in **Figure 3** and calculating the mobility ($\mu_{FET}$) according to the expression $\mu_{FET} = \frac{L}{C_i V_{SD} W} \frac{dI_{SD}}{dV_g}$ where L is the channel length (gap), W is the channel width, $V_{SD}$ is the source-drain bias, $C_i$ is the capacitance per unit area for 300 nm $SiO_2$ insulator, $I_{SD}$ is the source-drain current, and $V_g$ is the gate voltage [15]. Before ALD (**Figure 3a**), carrier mobilities were $5\times10^{-3}$ up to $4\times10^{-2}$ $cm^2/Vs$ for holes and $10^{-3}$ up to $10^{-2}$ $cm^2/Vs$ for electrons. However, after ALD (**Figure 3b**) the FET was dominated by hole currents with hole mobilities from 0.2 to 0.4 $cm^2/Vs$—a 10-times increase in hole mobility following alumina ALD. Both the increase in the doping and the increase in the carrier mobility contribute to the increased conductance of the HgTe CQD thin films following ALD.

 doi:10.20944/preprints202407.1429.v1



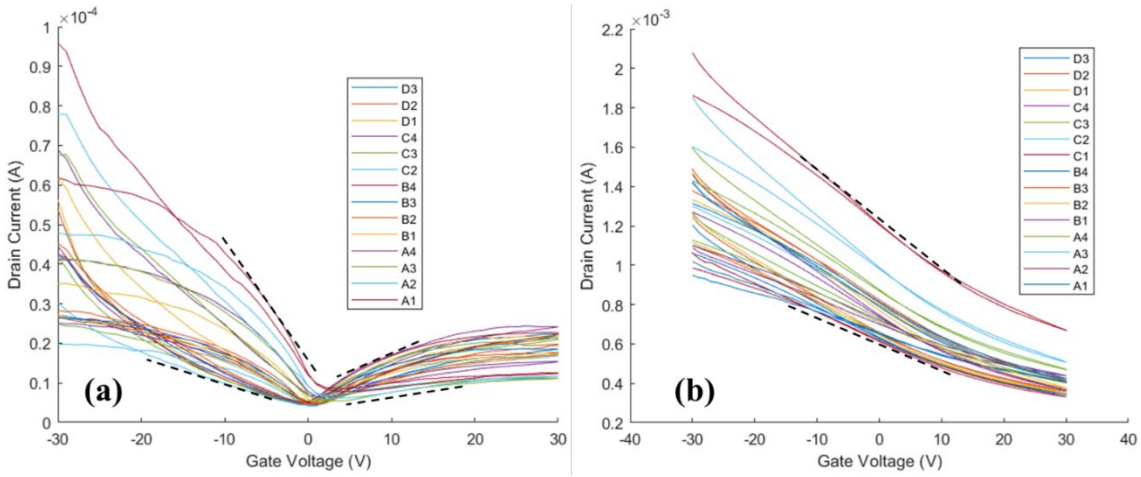


**Figure 3.** Transfer curves for HgTe colloidal quantum dot thin films measured at 1 V source-drain bias (a) before alumina ALD and (b) after alumina ALD. Black dashed lines indicate the maximum and minimum slopes taken to calculate the carrier mobilities.

From these observations, it is reasonable to conclude that alumina ALD coatings will consistently increase the p-type doping and carrier mobilities of HgTe CQD thin films. Compared to HgTe CQDs, prior works on Pb chalcogenides have higher carrier mobilities because of ALD in-filling, attributing the improvements to trap filling for alumina-coated Pb chalcogenides [7]. However, with respect to doping, Pb chalcogenides consistently showed less p-type and more n-type doping—that is, the opposite direction to the changes observed here for HgTe CQDs. The changes in doping for Pb chalcogenides have been attributed to acceptor state passivation by alumina ALD, thus reducing the p-type doping density [7]. By analogy then, alumina ALD on HgTe CQDs could have the effect of passivating hole traps, increasing acceptor states, and/or decreasing donor states. Alternatively, changes in the net surface dipole of the CQDs following from reactions with the ALD precursors during deposition may also explain the doping shifts of these materials [14]. From the perspective of the CQDs, these effects are functionally equivalent, causing the Fermi level to shift relative to the conduction and valence levels and shifting the doping of the system.

To better understand the possible impact of ALD on doping and mobilities of HgTe CQDs, n-type HgTe CQDs were synthesized as reported by Yang et al. and studied by FET measurements [9]. The n-type doping was achieved by transferring the HgTe CQDs from non-polar octane into polar N,N-dimethylformamide (DMF) in the presence of excess mercury chloride ($HgCl_2$). The HgTe CQDs were cleaned to remove excess polar ligands and re-dissolved in DMF. Thin-film backside-gated FETs were made using n-type HgTe CQDs, coated from DMF, to characterize their doping and mobility before and after ALD in-filling. From the previous discussion, it was reasonable to expect that the n-type HgTe CQDs would become increasingly p-type and the carrier mobilities would improve with ALD in-filling.

The transfer curve for the n-type HgTe CQD film without and with ALD is shown in **Figure 4**. In this case, before ALD (**Figure 4a**) the HgTe CQDs show only electron transport with carrier mobility of 0.3 to 0.5 $cm^2/Vs$ and minima of conductance at $V_g$ less than -5 V, which suggests lightly n-type doped films. Following ALD (**Figure 4b**), the minima of conductance shifted toward $V_g = 0$ V and hole currents were now measurable at negative gate voltages. Electron and hole mobilities following ALD were both between 0.1 to 0.3 $cm^2/Vs$ and comparable in magnitude to the electron carrier mobility before ALD. The shift in the conductance minima and the increase in the hole conductance were both consistent with decreasing n-type character of the film following alumina ALD in-filling.

 doi:10.20944/preprints202407.1429.v1



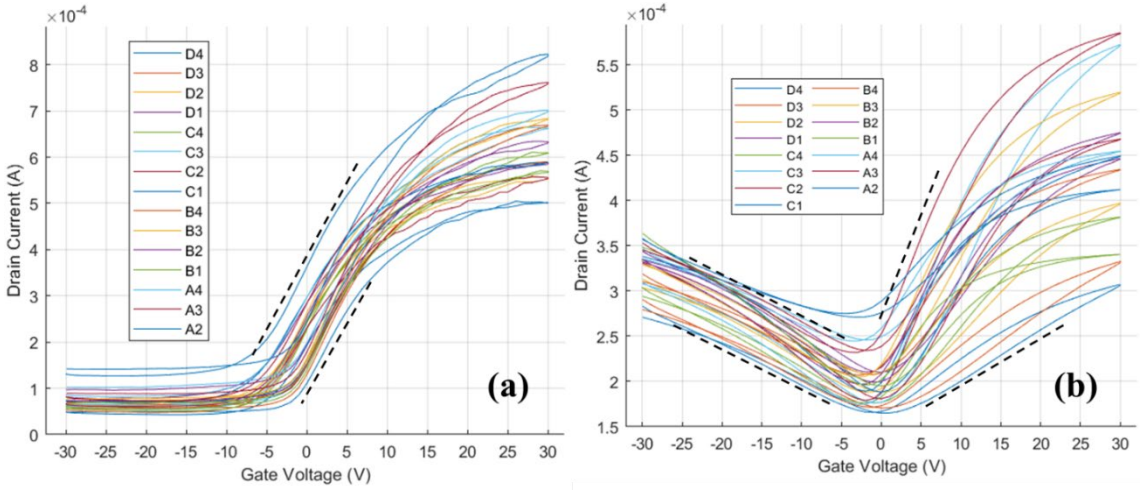


**Figure 4.** Transfer curves for n-type doped HgTe colloidal quantum dot thin films measured at 1 V source-drain bias (a) before alumina ALD and (b) after alumina ALD. Black dashed lines indicate the maximum and minimum slopes taken to calculate the carrier mobilities.

As in the previous case of p-type HgTe CQDs shown in Figure 3, ALD in-filling tended to decrease the n-type doping and increase the p-type doping of the HgTe CQD thin films. Contrary to the previous case however, the carrier mobilities were not improved, as evidenced by the comparable electron mobilities before and after ALD for the n-type HgTe CQDs. Furthermore, when p-type HgTe CQDs were prepared by phase exchange to polar DMF in a deficit of HgCl2 and then coated with alumina by ALD, similar results were observed (Supplementary Figure S3) with hole mobility effectively constant before and after alumina ALD. The impact of alumina ALD on carrier mobility was much less significant when HgTe CQDs were phase transferred to DMF. These observations may be explained by the differences in the processing of each of the HgTe CQD thin films investigated here.

**Conclusions:**

In conclusion, low-temperature alumina ($Al_2O_3$) atomic layer deposition (ALD) was demonstrated as a feasible approach to prepare conductive films of HgTe colloidal quantum dots (CQDs) with enhanced thermal stability against sintering. Thermal stability of the HgTe CQD thin films was established over the temperature range from 80°C to 160°C with minimal impact on its optical properties and conductance of thin films before and after baking. Field effect transistor (FET) measurements were used to study the impact of ALD on the electronic properties of the HgTe CQD films. Results from the FET measurements revealed that (1) carrier mobility was either preserved or improved and (2) doping generally shifts with decreasing n-type and increasing p-type character due to alumina ALD in-filling. The magnitude of these effects following ALD was found to be dependent on the process conditions used to prepare the HgTe CQD films. While these investigations into the electronic properties were not exhaustive, the results reported here motivate the need for a better understanding of the interaction effects between the CQD structure, surface chemistry, and ALD materials. Under optimized conditions then, it may be possible to engineer heterojunction and homojunction devices that are made thermally robust by ALD in-filling and passivation. A detailed understanding of how these factors interact and influence the electronic properties of CQD-ALD composites will be beneficial to engineer and manufacture robust CQD-based optoelectronic devices.

**Supplementary Materials:** The following supporting information can be downloaded at the website of this paper posted on Preprints.org. Figure S1: Temperature dependence of transfer curves for aggregated p-type HgTe CQD films through ALD coating and bakes; Figure S2: Absorption spectra of n-type HgTe CQD before and after ALD, before and after baking; Figure S3: Temperature dependence and transfer curves for phase

 doi:10.20944/preprints202407.1429.v1



transferred, p-type HgTe CQD; Figure S4: Temperature dependence of transfer curves for phase transferred, n-type HgTe CQD.

**Author Contributions:** Conceptualization, Matthew Ackerman; Data curation, Edward Malachosky and Matthew Ackerman; Formal analysis, Edward Malachosky; Funding acquisition, Matthew Ackerman; Investigation, Edward Malachosky; Methodology, Edward Malachosky, Matthew Ackerman and Liliana Stan; Project administration, Matthew Ackerman and Liliana Stan; Resources, Matthew Ackerman and Liliana Stan; Supervision, Matthew Ackerman and Liliana Stan; Validation, Edward Malachosky and Liliana Stan; Visualization, Edward Malachosky; Writing – original draft, Matthew Ackerman; Writing – review & editing, Edward Malachosky and Liliana Stan.

**Funding:** Work by Matthew Ackerman was supported in part by appointment with Chain Reaction Innovations (CRI) at the Argonne National Laboratory. CRI is sponsored funded supported by the U.S. DOE, Office of Energy Efficiency and Renewable Energy, Office of Science, and Office of Fossil Energy and Carbon Management as a part of the Lab-Embedded Entrepreneurship Program (LEEP). This research was specifically supported by the Advanced Manufacturing Office program. The fellowship program is administered by the Oak Ridge Institute for Science and Education (ORISE) for the DOE. ORISE is managed by ORAU under DOE Contract No. DESC0014664.

This research was partially funded by the National Science Foundation under Small Business Innovation Research Award No. 2112359.

**Data Availability Statement:** The original contributions presented in the study are included in the article/supplementary material, further inquiries can be directed to the corresponding author/s.

**Acknowledgments:** The authors thank C. Suzanne Miller and Dr. Ralu Divan at the Center for Nanoscale Materials for providing technical support and troubleshooting microfabrication capabilities throughout the duration of this work.

Work performed at the Center for Nanoscale Materials, a U.S. Department of Energy Office of Science User Facility, was supported by the U.S. DOE, Office of Basic Energy Sciences, under Contract No. DE-AC02-06CH11357.

Work by M.M.A. was supported in part by appointment with Chain Reaction Innovations (CRI) at the Argonne National Laboratory. CRI is sponsored funded supported by the U.S. DOE, Office of Energy Efficiency and Renewable Energy, Office of Science, and Office of Fossil Energy and Carbon Management as a part of the Lab-Embedded Entrepreneurship Program (LEEP). This research was specifically supported by the Advanced Manufacturing Office program. The fellowship program is administered by the Oak Ridge Institute for Science and Education (ORISE) for the DOE. ORISE is managed by ORAU under DOE Contract No. DESC0014664.

This material is based upon work supported by the National Science Foundation under Small Business Innovation Research Award No. 2112359.

**Conflicts of Interest:** Edward Malachosky and Matthew Ackerman are employed by and own stocks in QDIR, Inc. All authors had full access to all of the data in this study. The funding agencies had no role in the design of the study; in the collection, analyses, or interpretation of data; in the writing of the manuscript; or in the decision to publish the results.

## References:

1. Won, YH., Cho, O., Kim, T. et al.; Highly efficient and stable InP/ZnSe/ZnS quantum dot light-emitting diodes. Nature 575, 634–638 (2019).
2. Xufeng Ling, Jianyu Yuan, and Wanli Ma; The Rise of Colloidal Lead Halide Perovskite Quantum Dot Solar Cells. Accounts of Materials Research 2022 3 (8), 866-878
3. Nikolay S. Makarov, Daniel Korus, Daniel Freppon, Karthik Ramasamy, Daniel W. Houck, Andres Velarde, Ashray Parameswar, Matthew R. Bergren, and Hunter McDaniel; Minimizing Scaling Losses in High-Performance Quantum Dot Luminescent Solar Concentrators for Large-Area Solar Windows. ACS Appl. Mater. Interfaces 2022, 14, 26, 29679–29689.
4. J. S. Steckel *et al.*, "1.62$\mu$m Global Shutter Quantum Dot Image Sensor Optimized for Near and Shortwave Infrared," *2021 IEEE International Electron Devices Meeting (IEDM)*, 2021, pp. 23.4.1-23.4.4.

5. Li, Zhi, Ye Tian, Chao Teng, and Hai Cao. 2020. "Recent Advances in Barrier Layer of Cu Interconnects" Materials 13, no. 21: 5049.
6. Hye-Mi So, Hyekyoung Choi, Hyung Cheoul Shim, Seung-Mo Lee, Sohee Jeong, Won Seok Chang; Atomic layer deposition effect on the electrical properties of Al2O3-passivated PbS quantum dot field-effect transistors. Appl. Phys. Lett. 2 March 2015; 106 (9): 093507.
7. Yao Liu, Jason Tolentino, Markelle Gibbs, Rachelle Ihly, Craig L. Perkins, Yu Liu, Nathan Crawford, John C. Hemminger, and Matt Law; PbSe Quantum Dot Field-Effect Transistors with Air-Stable Electron Mobilities above 7 cm2V−1s−1. Nano Letters 2013 13 (4), 1578-1587.
8. R. W. Crisp, F. S. M. Hashemi, J. Alkemade, N. Kirkwood, G. Grimaldi, S. Kinge, L. D. A. Siebbeles, J. R. van Ommen, A. J. Houtepen; Atomic Layer Deposition of ZnO on InP Quantum Dot Films for Charge Separation, Stabilization, and Solar Cell Formation. Adv. Mater. Interfaces 2020, 7, 1901600.
9. Ji Yang, Huicheng Hu, Yifei Lv, Mohan Yuan, Binbin Wang, Ziyang He, Shiwu Chen, Ya Wang, Zhixiang Hu, Mengxuan Yu, Xingchen Zhang, Jungang He, Jianbing Zhang, Huan Liu, Hsien-Yi Hsu, Jiang Tang, Haisheng Song, and Xinzheng Lan; Ligand-Engineered HgTe Colloidal Quantum Dot Solids for Infrared Photodetectors. Nano Letters 2022 22 (8), 3465-3472.
10. Matthew M. Ackerman, Menglu Chen, Philippe Guyot-Sionnest; HgTe colloidal quantum dot photodiodes for extended short-wave infrared detection. Appl. Phys. Lett. 24 February 2020; 116 (8): 083502.
11. Todd H. Ballinger and John T. Yates, Jr.; IR Spectroscopic Detection of Lewis Acid Sites on Al2O3 Using Adsorbed CO Correlation with Al-OH Group Removal. Langmuir 1991, 7, 3041-3045.
12. Heshmat Noei, Hengshan Qiu, Yuemin Wang, Elke Loffler, Christof Woll, and Martin Muhler; The identification of hydroxyl groups on ZnO nanoparticles by infrared spectroscopy. Phys. Chem. Chem. Phys., 2008,10, 7092-7097.
13. Michel Primet, Pierre Pichat, and Michel V. Mathieu; Infrared study of the surface of titanium dioxides. I. Hydroxyl groups. The Journal of Physical Chemistry 1971 75 (9), 1216-1220.
14. Kwang Seob Jeong, Zhiyou Deng, Sean Keuleyan, Heng Liu, and Philippe Guyot-Sionnest; Air-Stable n-Doped Colloidal HgS Quantum Dots. *The Journal of Physical Chemistry Letters* **2014** *5* (7), 1139-1143.
15. Yao Liu, Markelle Gibbs, Craig L. Perkins, Jason Tolentino, Mohammad H. Zarghami, Jorge Bustamante Jr., and Matt Law; Robust, Functional Nanocrystal Solids by Infilling with Atomic Layer Deposition. Nano Letters 2011 11 (12), 5349-5355.